# In-situ imaging and computational modeling reveals that thiophene complexation with Co(II)porphyrin/graphite is highly cooperative.

Kristen N. Johnson<sup>+</sup>, Shammi Rana<sup>+</sup>, Bhaskar Chilukuri<sup>†</sup>, K.W. Hipps\*, and Ursula Mazur\*

Department of Chemistry and Materials Science and Engineering Program, Washington State University, Pullman, Washington 99163-4630, United States

† Department of Chemistry, Illinois State University, Normal, Illinois 61790, USA

Corresponding Authors: hipps@wsu.edu, umazur@wsu.edu

#### **Abstract**

Scanning tunneling microscopy (STM) was employed to quantitively investigate in-situ binding of 3phenyl thiophene (PhTh) to Co(II)octaethyl porphyrin (CoOEP) supported on highly ordered pyrolytic graphite (HOPG) in fluid solution. To our knowledge, this is the first single molecule level study of a complexation reaction between a metalloporphyrin and a sulfur base at the solution/solid interface and one of the few examples of thiophene coordination with a d<sup>7</sup> transition metal. Real time imaging experiments revealed that PhTh binds reversibly to HOPG supported CoOEP at room temperature. The coordination process increases with increasing PhTh concentration. The nearest-neighbor analysis of STM images indicates that the complexation reaction is cooperative. Since PhTh does not bind to CoOEP in solution, the STM results strongly suggest that the presence of HOPG is crucial to observe ligand binding and cooperativity in this system. Periodic plane-wave density functional theory (DFT) computations corroborate that PhTh has low binding affinity toward CoOEP in solution but predict that the ligand can adsorb to CoOEP/HOPG through coordination with S atom or interact through noncovalent  $\pi$ - $\pi$  bonding with the porphyrin chromophore. Three possible structures were considered and DFT theory used to calculate binding energies and free energies. In solution and on the HOPG surface both a  $\pi$ - $\pi$  and a  $\eta^1(S)$ configuration have similar computed energies. The  $\eta^1(S)$  structure shows the largest stabilization in going from the vapor to adsorbed on HOPG. We also show that statistical analysis of nearest neighbors is more sensitive to cooperative binding than is fitting with the Temkin or Langmuir isotherm. The implication is that isotherm fitting alone is insufficient for identifying cooperative binding on surfaces.

# Introduction

Thiophene (SC<sub>4</sub>H<sub>4</sub>) and thiophene derivatives are heterocyclic molecules that are known to form complexes with transition metals <sup>1,2,3,4</sup> and also react with metals supported on surfaces. <sup>5,6</sup> Although thiophene coordination chemistry is best understood in the context of hydrodesulfurization (HDS)

homogeneous <sup>7,8</sup> and heterogeneous catalysis, <sup>7,9,10,11</sup> thiophenic compounds have also been exploited in applications ranging from biological, <sup>12</sup> pharmacological, <sup>13,14</sup> sanitizing, <sup>15</sup> to corrosion resistance, <sup>16,17</sup> chemical sensing <sup>18,19</sup> and in optoelectronic devices. <sup>20,21</sup>

Thiophenes, are very weak sulfur-donor ligands compared to alkyl or aryl-alkyl sulfides. Their aromatic character accounts for several different coordination modes in homogeneous transition metal complexes that include a direct bond between the sulfur atom and the metal  $(\eta^1(S))$  or the carbon atoms of the  $\pi$  ring system and the metal ( $\eta^2$ ,  $\eta^4$ , and  $\eta^5$ ).<sup>1,2,22</sup> The binding geometry of the thiophenes is generally modified by steric and electronic properties of other ligands attached to the metal center.<sup>23</sup> Accurate knowledge of thiophenes coordination chemistry and structural details in homogeneous metal complexes has been obtained from spectroscopic, crystallographic and density functional theory (DFT) based mechanistic studies. 1-25 There are, however, very few similarly detailed studies of binding to metals and metal complexes in heterogenous environments involving solid supports. <sup>5</sup>

Current keen interest in thiophenes reactive adsorption to metal complexes supported on surfaces is limited by a dearth of information about the local structure of the molecules under reaction conditions. To date, studies of thiophene binding to transition metal complexes supported on solid substrates has been limited (vide infra). 19,26 Particular attention has been focused on in-situ HDS studies monitoring the reaction of thiophenes with molybdenum, tungsten, rhenium with Co, Mg or Ni promoters adsorbed on metal oxides (Al<sub>2</sub>O<sub>3</sub>, SiO<sub>2</sub>) and graphite. 9,27,28,29,30 Studies involving catalyst characterization, thiophene adsorption, and reaction dynamics employed X-ray,<sup>31</sup> IR,<sup>32,33</sup> NMR,<sup>34,35</sup> and density functional theory (DFT) methods. 36,37 Proposed thiophene binding modes to the different metal centers on the surface included  $\eta^1(S)$  and η<sup>5</sup>(C=C) coordination.<sup>33</sup> However, because the catalyst surface is complex, the mode(s) of thiophene absorption and reaction dynamics are still not well established. Furthermore, while the above analysis methods can be quite powerful, they can only provide average structural information when many adsorption sites are present.

Scanning tunneling microscopy, STM, a highly resolving analysis technique, is particularly wellsuited for studying adsorption and reactions on

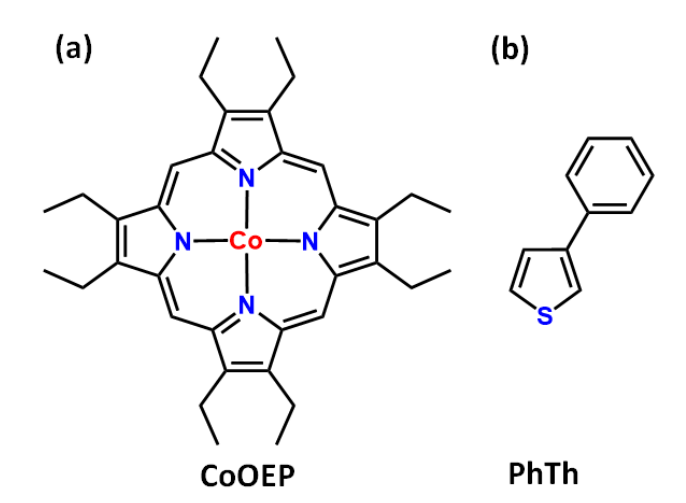


**Figure 1:** Molecular structure of cobalt(II)octaethyl porphyrin (CoOEP) and 3-phenylthiophene (PhTh) molecules.

surfaces and interfaces. To date, it has been applied primarily to investigate self-assembly of thiophenes on gold and silver substrates.<sup>6,38,39</sup> A recent STM report identified adsorption sites of thiophene on MoS<sub>2</sub> nanoparticles supported on Au(111) to be at the Mo-edge sites. Because the relative sizes of individual thiophene molecules and S atoms at the Mo-edges appeared to be similar they could not be uniquely identified.<sup>5</sup>

Our work in surface-based coordination chemistry capitalizes on STM single molecule level sensitivity to gain quantitative insight into the identity and distribution of adsorbate reactive sites, ligand binding dynamics, and reaction mechanisms. We conduct STM experiments at the solution/solid interface in-situ at variable temperatures and pressures. Several STM studies reported by us, and others have effectively demonstrated in-situ chemistry and reaction dynamics of heterocyclic ligand coordination to metal complexes (porphyrins and phthalocyanines<sup>40,41</sup>) adsorbed on solid supports at the solution/solid interface. Some of these reports confirmed that axial ligation can be reversible, and, furthermore, that the electronic properties, reactivity, and cooperativity (nonadditive interactions) of the adsorbed complex be modulated by the underlaying substrate. 42,43,44 The binding reactions of imidazole to NiOEP<sup>45</sup> and 1-phenylimidazole (PhIm) to

CoOEP<sup>46</sup> proceeded at room temperature because of charge donation from the underlying graphite substrate to porphyrin.<sup>47</sup> The presence of HOPG was also crucial to observe positive cooperativity for both 4-methoxypyridine<sup>43</sup> and PhIm binding to CoOEP<sup>46</sup> at the solution/solid interface. Similarly it was observed that 3-nitropyridine coordinated more strongly to Zn(II) 5,10,15,20-meso-tetradodecyl porphyrin (ZnTDP) supported on HOPG surface than porphyrin dissolved in solution.<sup>48</sup>

There have been only a few examples of metalloporphyrins binding to thiophene. Cobalt tetraphenyl porphyrin, CoTPP, and Ru(II)TPP were shown to bind gaseous thiophene by modified quartz microbalance. Blectron paramagnetic resonance spectroscopy confirmed a 5-coordinate thiophene CoTTP complex at low temperature in toluene solution. Fe(II)tetra(pentafluorophenyl) porphyrin electrografted onto carbon nanotubes and axially coordinated with thiophene produced an increased rate of oxygen reduction compared with the porphyrin on nanotubes alone. <sup>49</sup>

In this work we exploit the in-situ capabilities of STM in combination with complementary DFT studies for quantitative investigation of 3-phenyl thiophene binding to CoOEP (Figure 1) adsorbed on a graphite support in a solution environment. To the best of our knowledge, this is the first STM report of a thiophene ligand coordination metalloporphyrin at the solution/solid interface. Collective results from experimental computational studies allow us to rationalize cooperative PhTh-CoOEP/HOPG interactions and the importance of the substrate to facilitate and strengthen the thiophene-CoOEP bond. Calculated PhTh-CoOEP/HOPG structural models and their relative binding energies support the prominent role of the HOPG substrate in determining the most stable adopted geometry of the surface complex.

## EXPERIMENTAL SECTION

**Materials.** 2,3,7,8,12,13,17,18-octaethyl-21H,23H-porphine cobalt(II) (CoOEP) and 3-Phenylthiophene (PhTh) were purchased from

Sigma-Aldrich (St. Louis, MO, USA). 1-phenyloctane (>98.0%) was obtained from TCI America (Portland, OR, USA). Toluene (ACS grade or J.T. Baker, Ultra Resi-Analyzed) was acquired from Fisher Scientific (Waltham, MA, USA). All chemicals were used without further purification. HOPG substrates used were 1 cm² in size and obtained from SPI (grade 2; West Chester, PA, USA) or TipsNano Co (ZYA quality; Tallinn, EE). STM tips were mechanically cut from Pt/Ir wire (California Fine Wire Co., Grover Beach, CA, USA; 80:20 Pt/Ir, 0.011 in. diameter).

STM Sample Preparation and Imaging. A  $20 \mu M$ CoOEP stock solution was prepared by dissolving solid CoOEP in phenyloctane solvent. PhTh octyl benzene solution was in the millimolar Both CoOEP and PhTh concentration range. solutions were stored in the dark at room temperature. Molecular Imaging PicoSPM equipped with a 1 µm STM scanner and environmental chamber (for a controlled atmosphere) was employed for acquiring STM images in constant current mode at bias voltages ranging from +0.6 to +0.8 V and a set-point current of 20 pA. To prepare samples for STM imaging, first 20 µL of 20 µM of CoOEP solution was deposited on freshly cleaved HOPG substrate which was then mounted in a custom-made solution 500 µL Teflon cell fitted with a Kalrez o-ring (McMaster-Carr, Elmhurst IL, USA). The sample was then placed in the environmental chamber and purged with 2.5 standard cubic feet per hour (scfh) argon gas for 45 minutes.<sup>50</sup> After purging, the gas flow was reduced to 1 scfh and maintained throughout the imaging experiment. After confirming that a satisfactory CoOEP monolayer was formed, PhTh (10 µL of appropriate concentration) was added to the solution cell already containing CoOEP. The mixture was allowed to equilibrate for at least three hours before imaging. Final [CoOEP] and [PhTh] in the solution cell were calculated based on the volumes and concentrations of the porphyrin and ligand added.

Image Analysis and Statistics. STM image analysis was carried out using SPIP (Image

Metrology A/S, Lyngby, DK). For calculating the fraction of dark molecules and dark nearest neighbors from experimental data, a Matlab script was used, available in an online repository at https://github.com/kristen-johnson/STM-imagemanip-count. Typically, 90 nm × 90 nm STM images were used, which contained, on average, ~5000 surface adsorbed CoOEP molecules each. Images were fit with a grid such that each grid cell contained a single molecule. The average apparent height variance,  $\sigma^2 = \left[\sum (x_i - \bar{x})^2\right]/(n-1)^2$ , was then determined within each cell and these values were used to create a histogram of heights. Inspection of images showed two different types of molecules in each image: (1) unligated, bright molecules; (2) ligated, dark molecules. Threshold values were set and the average apparent height variance within each grid cell was compared with the thresholds to categorize the molecule within the cell and facilitate counting of each type of molecule. Using average height variance within each cell to create histograms provided a reduced rate of false positive results compared with mean apparent height values alone. Overall, the coverage or ratio of ligated molecules was calculated by equation 1. The location of ligated CoOEP molecules in the grid was also used to determine the distribution of bound nearest neighbors. In the pseudo-hexagonal lattice, all CoOEP have 6 nearest neighbors. For molecules on the edge of the images some of these neighbors are out of view, and data for all neighboring molecules is not available. In these cases, edge molecules are counted as potential neighbors for the inner molecules but were not themselves included in the distributions.

Computational Methods. Computations are performed with periodic density functional theory (DFT) using Vienna Ab-initio Simulation Package (VASP)<sup>51,52</sup> version 6.2.0. or with the program Gaussian 16.<sup>53</sup> The Gaussian DFT calculations were performed using both the B3LYP and the B3LYP-GD3 functional. A 6-311G basis was used on H, C, and N, the 6-311++G(d,p) basis on S, and the 6-311++G(2d,p) basis functions on Co. All Gaussian calculations

were made on single molecules in the gas-phase or in a solvent using the SCRF model with the SMD option.<sup>54</sup> A tilted  $\eta^1(S)$  configuration and  $\pi$  bonded configuration were found to be most stable and close in free energy of formation.

The VASP code uses the projector augmented wave (PAW) method<sup>55,56</sup> to describe the core electrons and valence-core interactions. We used the GGA optB88vdw functional<sup>57,58</sup> with the PAW optimized potentials. The electronic wavefunctions were determined at the Gamma  $(\Gamma)$  point in the irreducible Brillouin zone. A plane wave (PW) cut off energy of 550 eV was used for all simulations. For the HOPG and adsorbate-HOPG systems, Methfessel-Paxton smearing was used to set the partial occupancies for each wave function with a smearing width of 0.2 eV. For the isolated molecular systems Gaussian smearing was used with a width of 0.04 eV. All the geometries were fully optimized up to 0.001 eV energy convergence and less than 0.02 eV/A forces. The choice of our DFT methodology, plane wave cutoff energies and kpoint choice were based on previous periodic DFT simulations of similar systems of type<sup>59-63</sup> and size<sup>64</sup>. VASP calculations were performed on species adsorbed to 2-layer graphite and on the same species in the gas phase.

# RESULTS AND DISCUSSION

PhTh binds to CoOEP adsorbed on HOPG. Unlike its close nitrogen base analog 1phenylimidazole, 65 3-phenylthiophene did not bind to CoOEP in solution (toluene or phenyloctane) at 25 °C even at concentrations exceeding 100-fold that of the metal porphyrin (see Figure S1 in Supporting Information). This allows us to estimate that  $\Delta G$  for formation in phenyloctane is greater than +0.4 kcal/mole. This result was expected since thiophene is known to coordinate to at most weakly transition metal ions. What was surprising is that the thiophene reacted with CoOEP absorbed at the phenyloctane/HOPG interface at room temperature. This reaction was monitored in real time under controlled conditions (vide infra). When the ligand was added to previously examined well-ordered

CoOEP monolayer (pseudo hexagonal), two discernible types of molecules were observed, bright and dim, as depicted a representative STM image in Figure 2a. Figure 2b-c provides insights into the data analysis method. The bright features are attributed to the unreacted CoOEP molecules where tunneling through the half-filled d<sub>z</sub><sup>2</sup> orbital of the Co(II) produced bright molecular centers consistent with previous reports.<sup>47</sup> The dim sites are assigned to the PhTh–CoOEP complex and have

apparent heights less than half that of the unbound metal porphyrin due to a reduced number of available states near the Fermi surface. It is the observed attenuated conductivity in the ligated species which allows differentiation between unligated and ligated cobalt porphyrins. It is worth noting that neither time of exposure or order of mixing significantly affects our results (Figure S2, S3, and S4). Reported STM images of ligands such as oxygen, <sup>36,66</sup> imidazole, <sup>28</sup> 1-phenylimidazole, and

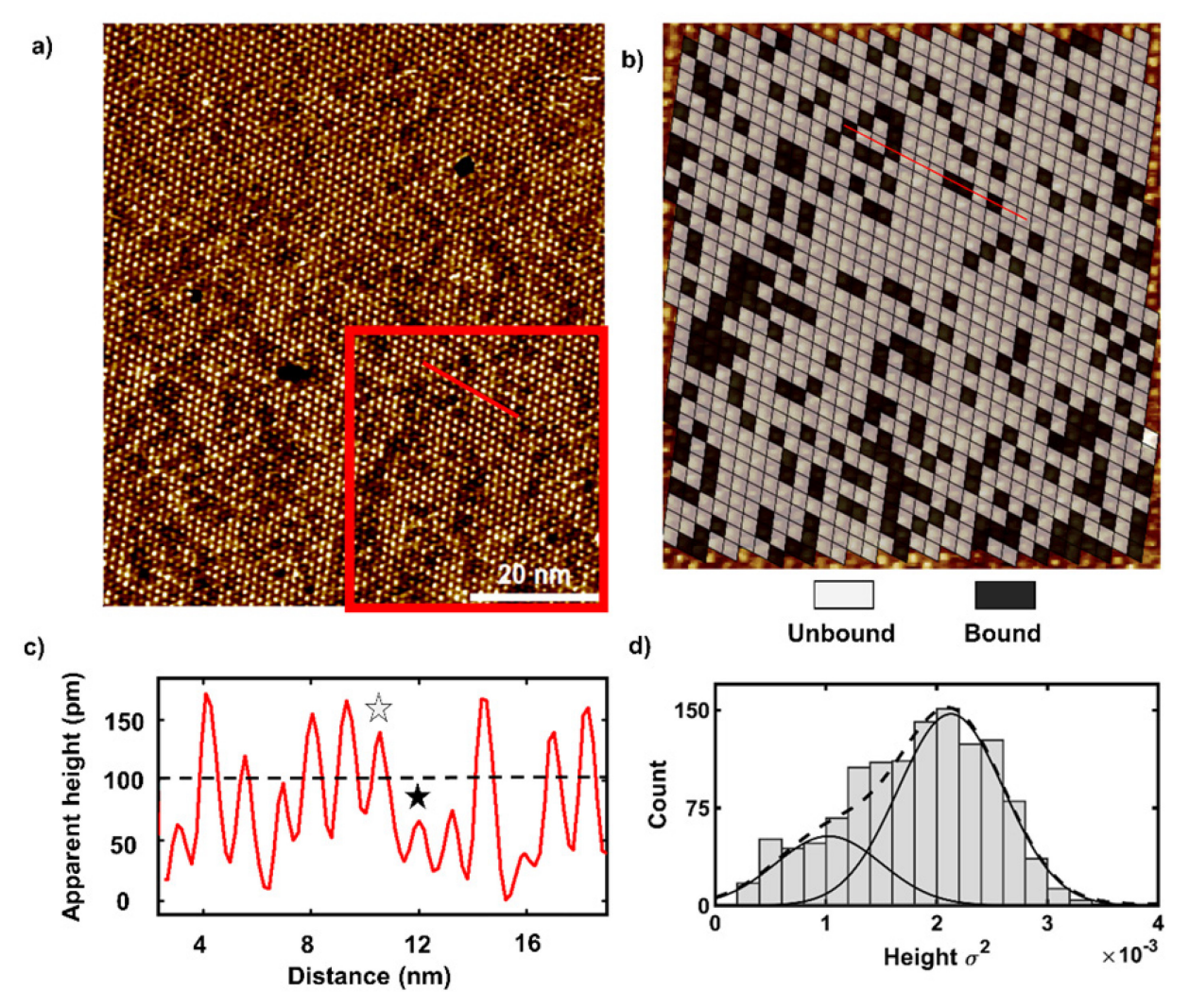


**Figure 2.** (a) Representative STM image of a monolayer of  $1.3 \times 10^{-5}$  M CoOEP, at the 1-phenyloctane/HOPG interface after addition of PhTh (0.1 M). Image was acquired using a bias voltage of +0.6 V and 10 pA set point, under argon atmosphere, at room temperature. (b) A section of image (a) enlarged and overlaid with color coordinated grid identifying the ligation state of each molecule as determined from apparent height threshold values. (c)Cross-sectional profile along the red line in (a) and (b) showing an apparent height threshold (dashed line) with 2 types of molecule state classifications identified by stars with the same color code same as in (b). (d) Apparent height distribution from image (b) fit to two Gaussian functions with equal width.

3-MeOPy, axially coordinated to cobalt porphyrins at the solution/HOPG interface all exhibited reduction in the conductivity at the metal center. 47,45

Closer examination of Figure 2a reveals regions of clustering of ligated CoOEP molecules in the STM image. To capture the true experimental average of the PhTh-CoOEP species, multiple large scale STM images (~100 nm<sup>2</sup>) were used in calculating surface coverage of the ligated (dark) sites. Significant local grouping produces an inhomogeneity in the ratio of observed ligated molecules which is obvious in small scale images (<50 nm). The advantage of using large scale images is increased reproducibility in the observed average number of reacted surface sites. The disadvantage of using sizable STM images is potentially introducing counting errors in manual tallying of a very large number of molecules (~5000) per image. To achieve better and more systematic counting accuracy as well as reduction in time required for manual counting, a mathematical routine in MATLAB was developed and used to count dark and bright molecules in STM images. The MATLAB routine cataloged each molecule in the image by comparing its apparent height variance to a threshold value. Molecules were classified as PhTh-CoOEP adducts if their height was below the threshold and classified as free CoOEP when the height was above the threshold, see figures 2b and 2c. The bound molecule coverage,  $\theta$ , in an image was then calculated by using equation 1.

$$\theta = \frac{PhTh - CoOEP \ molecules}{\# \text{total CoOEP molecules}} \tag{1}$$

To verify the reliability of the 'threshold' calculation of coverage of ligated molecules, we

compared the results with a second method involving fitting the height histograms to two Gaussian functions. The variance of apparent height of the molecules fits well to two Gaussian functions where the peak with lower mean position corresponds to the ligated molecules and the other peak corresponds to the free CoOEP molecules. The ratio of areas under each curve was considered to be the coverage ratio,  $\theta$ , of each type of molecule in the images.

Two different methods for fitting Gaussian functions to the apparent height distributions were used because the significant overlap in the peaks made finding unique, reproducible fits to the distribution difficult. The first method fits the free CoOEP peak with a single Gaussian function first and then subtracts the fitted function from the total distribution and fits the residual with a second single Gaussian. An example of applying this method is shown in Figure 3. Because the results depend slightly on where the initial peak cut-off is set, a second method for fitting Gaussian functions was used, one that did not require a human eye to decide on threshold values or on a cut-off value. In this second method, the average apparent height distribution is fit to two Gaussian functions that are constrained such that both must have equal width. The assumptions here are that there are two population of molecules present and that the width of the distribution is determined by the variation in path of the tip over a particular molecule and the fluctuations of solvent molecules between tip and surface. An example of this method is shown in Figure 4. The peak positions are not constant between samples and depend strongly on the

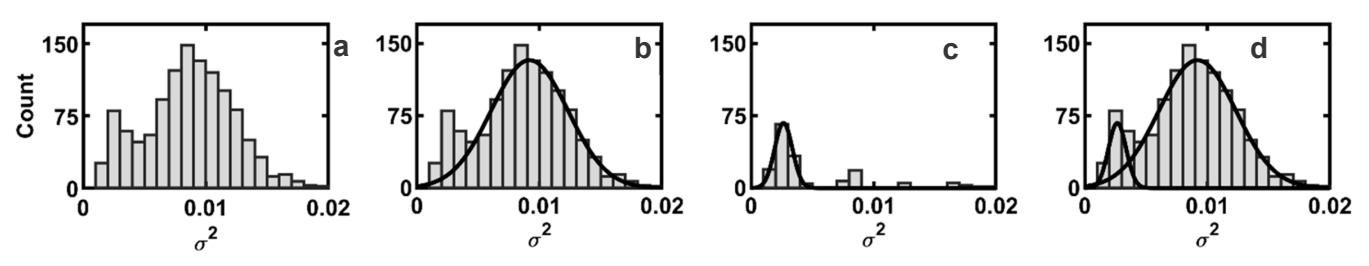


**Figure 3.** Example of Gaussian fit method 1. (a) The average apparent height distribution for a sample with 100 mM PhTh concentration. (b) The distribution with apparent height greater than 120 pm fit to a single Gaussian function which corresponds to the free CoOEP molecules. (c) Shows the residual distribution after subtracting the fitted function shown in 4b from the total distribution shown in 4a and again fitting with a single Gaussian function. This peak corresponds with the ligated CoOEP molecules. (d) Shows the total distribution with both Gaussian fits overlaid. The area ratio for the PhTh–CoOEP adduct peak is 25.5%.

**Table 1:** Comparison of PhTh–CoOEP adduct coverage values  $\theta$ , at varying PhTh concentration using three different data fitting methods.

	Adduct coverage (θ)						
[PhTh] (mM)	Threshold count	Gaussian fit method 1 (Consecutive fits)	Gaussian fit method 2 (Equal width)				
0	$0.1 \pm 0.005$	-	-				
1	$0.03 \pm 0.01$	-	-				
10	$0.075 \pm 0.02$	$0.065 \pm 0.03$	$0.06 \pm 0.02$				
50	$0.15 \pm 0.02$	$0.13 \pm 0.03$	$0.16 \pm 0.02$				
100	$0.23 \pm 0.03$	$0.22\pm0.04$	$0.25 \pm 0.05$				

sharpness of the STM tip. The area ratio, however, is reproducible across samples at equal PhTh concentrations. Both methods failed when coverage was less than 5% due to few instances of bound molecules entering into the histograms. The

As PhTh concentration is increased, the ratio of ligated CoOEP in the monolayer also increases. At each concentration, at least three 90x90 nm images were used to determine the PhTh–CoOEP coverage ratio by each method. This is ~ 15,000 CoOEP molecules at each concentration.

of PhTh binding CoOEP **Dynamics** monolayer. Consecutive STM scanning of the same area of the sample over time shows 'blinking,' i.e. molecules appeared to change from bright to dark and vice-versa. This contrast shift in the apparent height is due to deligation (dark to bright) and ligation (bright to dark) reactions of CoOEP with PhTh. The blinking indicates the dynamic and reversible nature of ligand binding to porphyrin at the solution/solid interface. An example of the transition is shown in Figure 5, with deligation transitions denoted with red circles, and ligation transitions denoted with green circles. CoOEP molecules that remained in the ligated state are

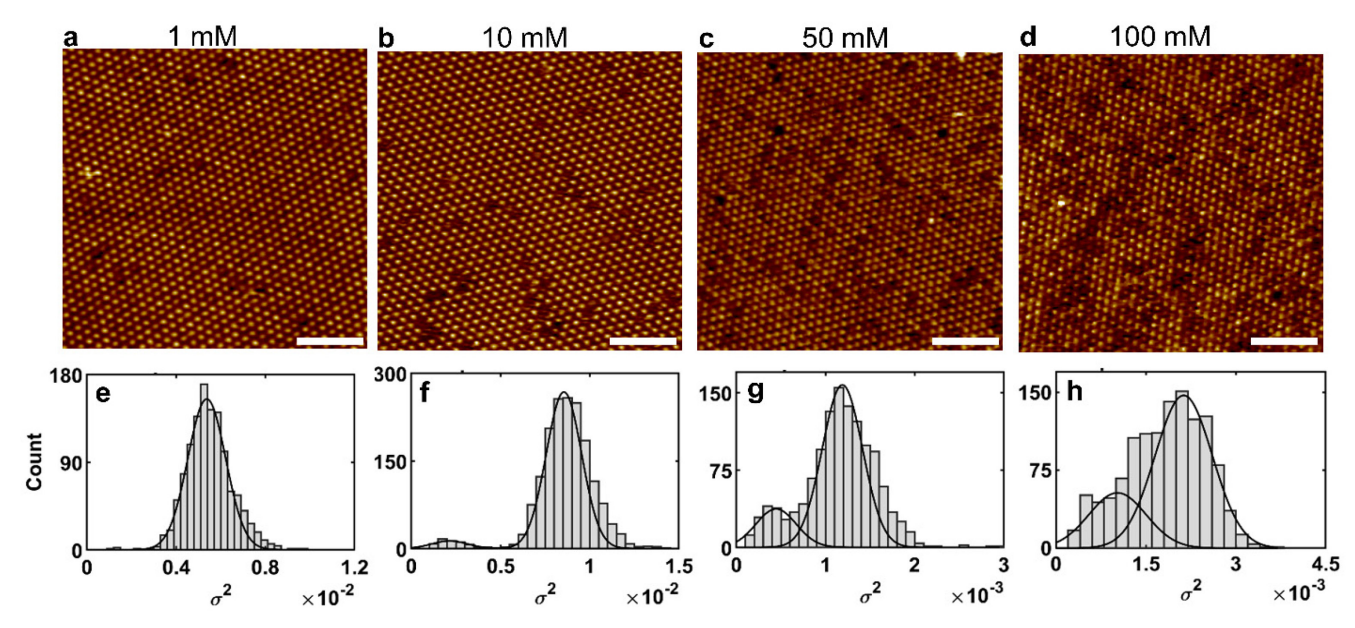


**Figure 4.** STM images with varying PhTh concentrations (1-100 mM) and CoOEP collected at +0.6 V and 10 pA (a-d). Graphs (e) to (h) show the corresponding variance  $\sigma^2$  in apparent height distributions for each molecule in the images fit with two Gaussian functions of equal width. The area ratio for the shorter peak, corresponding with the ligated molecules, increases from <5% to 20%. CoOEP concentration is 13  $\mu$ M in all images and PhTh concentration is 1 mM, (a) and (e); 10 mM, (b) and (f); 50 mM, (c) and (g); 100 mM, (d) and (h).

results of all three methods for determining the percentage of ligated CoOEP in each image at various PhTh concentration are shown in Table 1.

marked with white circles. Although the molecules change state over time the average ratio of ligated

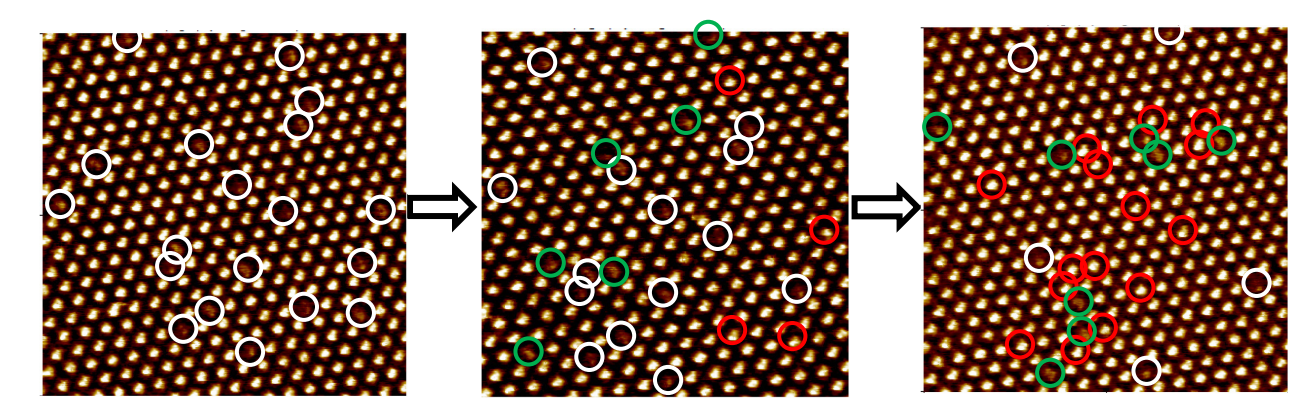


**Figure 5:** Consecutive STM images of CoOEP at phenyloctane/HOPG interface with 10 mM PhTh concentration. Images were collected sequentially at a speed of 63 s/image. In the first image all PhTh/CoOEP adduct molecules are denoted by white circles. In the next images molecules that change state from free CoOEP to PhTh bound with green circles and molecules that transition from ligated to free are denoted with red circles. The coverage in the images is 5.5%.

molecules remains constant in subsequent images, signaling the system is in dynamic equilibrium.

Having established that the system is at equilibrium, we can use the concentration and temperature dependence of the average coverage to determine thermodynamic properties of the system. Concentration dependent images were collected from 0 to 100 mM in [PhTh]. The concentration dependence of the coverage data fit well to the Langmuir isotherm, where  $\theta$  is the surface coverage. The Langmuir isotherm is given by:

$$[PhTh] = \frac{\theta}{(1-\theta)K} \tag{3}$$

where [PhTh] is the ligand concentration in solution and K is the equilibrium constant with standard state of 1 mole/L of PhTh and  $\theta$ =1/2. Plotting  $\theta$ /(1- $\theta$ ) versus the concentration of PhTh yields the data points shown in Figure 6, where the three methods of counting described earlier were used to generate the data points. K, the equilibrium constant, is the slope of the line. The equilibrium constant then is used to determine a  $\Delta G$  from the relationship  $\Delta G$  = -RT  $\ln(K)$  where R is the gas constant and T is temperature, 295 K. The average value of K from Figure 6 is 2.6, yielding  $\Delta G$  = -0.6 kJ/mole.

Binding of PhTh to CoOEP/HOPG is cooperative. The Langmuir isotherm assumes that all unoccupied sites on a surface are equally likely

to be occupied independent of coverage. That is, it assumes non-cooperative behavior. There are models for cooperative adsorption (where the heat or free energy of adsorption per site varies with coverage) and the Temkin model<sup>67,68</sup> is often used. In the Temkin model, the heat of adsorption varies as  $\Delta H = \Delta H^0 (1 + \alpha \theta)$ , and  $\alpha \Delta H^0 = \Delta \Delta H$ , the change in enthalpy of adsorption between the first and last molecule to adsorb. However, at low coverages unless the cooperativity is very strong, the variation in the average adsorption energy with coverage will be small and the Langmuir isotherm may yield satisfactory fits to cooperative systems. This can be seen in Figure 6, where the Temkin isotherm is plotted for  $\Delta\Delta H = -1.0$  kcal/mole and K = 2.0. This represents an increase in heat of adsorption by about 5% in our case.

An alternative method to analyze cooperativity in ligand binding is through nearest neighbor analysis. In this method, the distribution of bound molecules is determined and compared to the number of random events, modeled with a binomial distribution, where probability is equal to the surface coverage in the image. The nearest neighbor method will quantify the degree of clustering of ligated molecules in the CoOEP monolayer. A higher than predicted degree of clustering relative to a random distribution of bound molecules will be an indicator of increased probability for adjacent

ligated molecules. In the current case, demonstrating that the binding of PhTh to CoOEP is in fact cooperative.

The nearest neighbor distribution was calculated twice for each STM image using the result from the threshold counting method. A total of 12 representative images for each ligand concentration were used. Each image contained approximately 1125 molecules. An increase in the number of pairs and higher order clusters of bound molecules than expected in the random distribution case was observed for the same coverage with each ligand concentration employed. An example 10×10 nm<sup>2</sup> STM image section and associated histogram comparing the experimental to random distributions for 100 mM PhTh concentration are shown in figure 7a and 7b, respectively. The histogram of experimental and theoretical distribution of ligated nearest neighbors indicates a larger fraction of ligated neighbors of greater than 2 cluster size compared with the random prediction, shifting the distribution toward higher numbers of nearest neighbors ligated to PhTh. We attribute the difference to positive cooperativity in binding (more negative heat of adsorption for adjacent binding). With this molecular system the cooperative effects are easily observed and the increase in observed higher order clusters persists even in the lowest concentration of PhTh employed.

The Kolmogorov-Smirnov (KS) test can be used to test whether these distributions are statistically different. This test compares the absolute maximum distance between the experimental and expected cumulative probability distributions, Figure 7c, and compares the result to a critical value. The KS test uses the null hypothesis that there is no difference between the experimental distribution and the expected, random distribution. If the test statistic is less than the critical value the null hypothesis is accepted. The difference between the KS test statistic and critical values for the 95% confidence level are shown in Figure 7d, the null hypothesis is rejected for all concentrations (n = 406, 982, 1847, and 3477 for PhTh concentrations

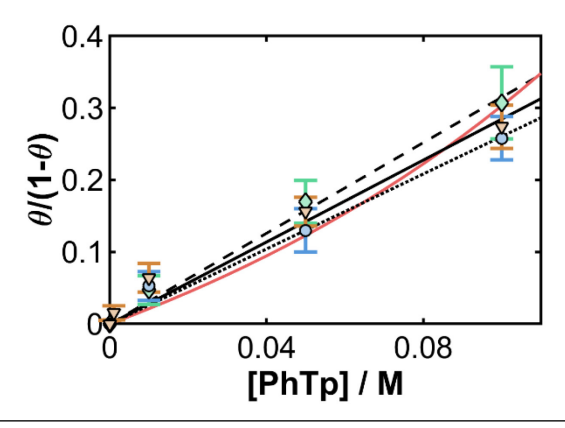


**Figure 6.** Langmuir isotherm fits for three methods used for determining the PhTh/CoOEP ratio,  $\theta$ . solid curve ( $\neg \nabla$ -), threshold count; dotted curve ( $\neg \nabla$ -), Gaussian method 1; dashed curve ( $\neg \nabla$ --), Gaussian method 2. A Temkin isotherm is shown in red.

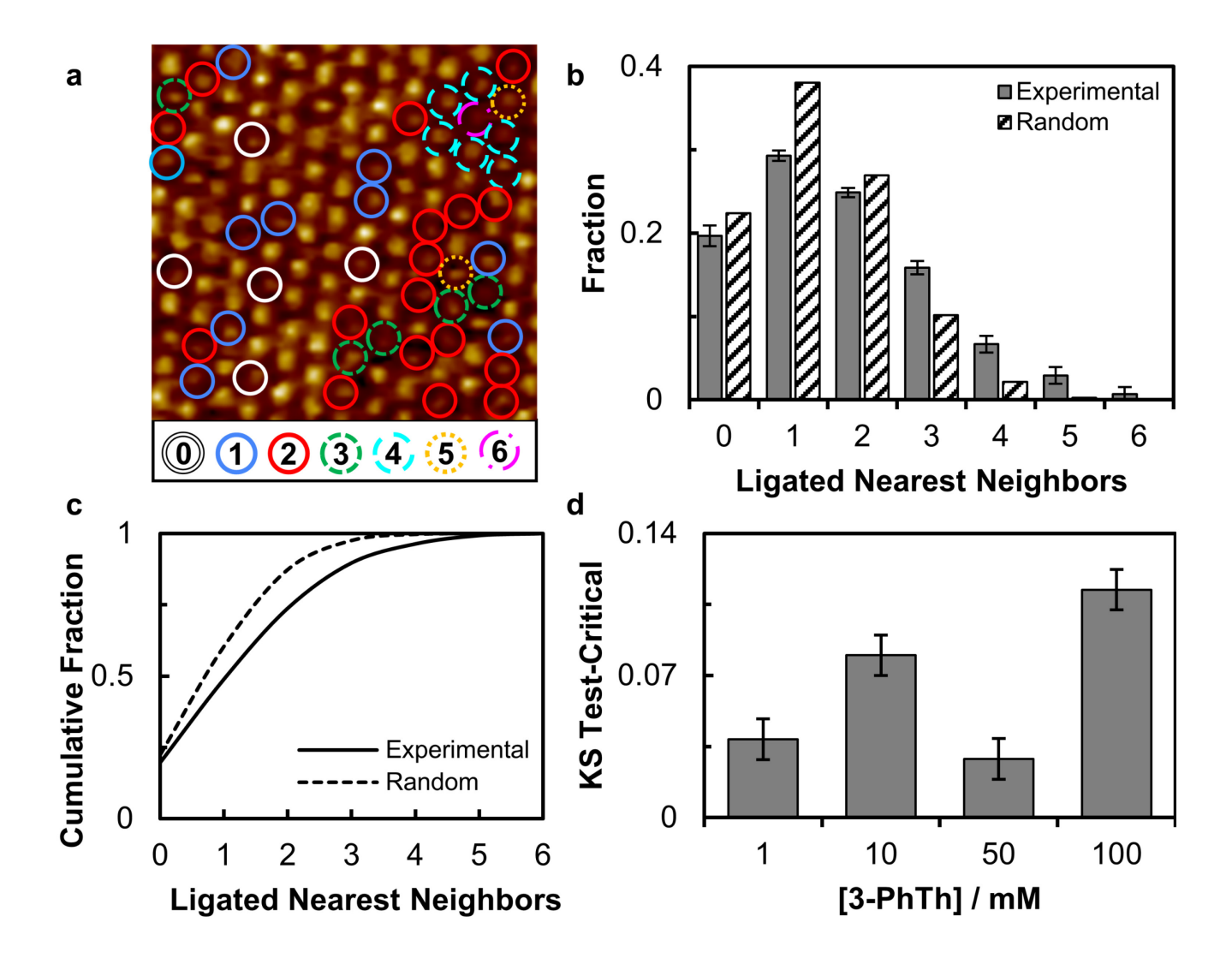


**Figure 7:** Nearest neighbor analysis results. (a) A  $10 \times 10$  nm² segment of typical STM image with overlaid color-coded rings showing the number of PhTh–CoOEP adduct nearest neighbors, PhTh concentration is 100 mM and  $\theta = 25\%$ . (b) Histogram comparing the ratio of number of ligated nearest neighbors experimentally observed (solid bar) with the ratio of nearest neighbor molecules predicted by the binomial distribution (striped bar) at 100 mM PhTh concentration. (c) Plot of cumulative fraction for random (dashed) and experimental (solid) distributions for 100 mM PhTh concentration. (d) Chart showing the difference between the KS test statistic and critical values for four different PhTh concentration. Test statistics are 0.11, 0.12, 0.06, and 0.13 while critical values are 0.07, 0.04, 0.03, and 0.02 for 1, 10, 50 and 100 mM PhTh respectively.

1, 10, 50, and 100 mM). These results strengthen the conclusion that the binding of PhTh to CoOEP is cooperative in nature. Note that for PhTh–CoOEP coverages less than 0.12, few images had cases where molecules had five or six ligated nearest

neighbors, which is the reason fewer number of data points in the scatter plots.

We believe that the observes cooperativity is mediated by the surface. Our recent paper on a similar complex showed through DFT calculations

**Table 2:** Energies and Free energies of formation (kcal/mole) of PhTh bonding to CoOEP free in vapor, in phenyloctane solution or adsorbed on HOPG. The Co-S and closest Co-C distances are given in Angstroms for structures where it is appropriate. Final optimized structures are presented in Figure 8.

_	Vapor	Vapor Phase				In PhO			
Nearest Initial Configuration	$\Delta E_f^0$	$\Delta G_{\mathrm{f}}$	R(Co-S)	R(Co-C)	$\Delta E_f^0$	$\Delta G_{\mathrm{f}}$	R(Co-S)	R(Co-C)	
B3LYP									
$\eta^1(S)^{TILT}$	-0.9	7.2	3.41		-0.8	10.4		4.43	
π-π	-1.4	7.0		5.08	-0.8	7.7		4.88	
$\eta^1(S)^{UP}$	-0.9	6.9	3.41		-0.9	7.7		4.32	
B3LYP-GD3									
$\eta^1(S)^{TILT}$	-18.0	-4.3	2.96		-14.8	-3.6	3.09		
π-π (meso)	-21.8	-7.3		3.35	-16.9	-1.1		3.35	
π-π (β)	-22.3	-6.9	3.38		-17.8	-4.6		3.49	
$\eta^1(S)^{UP}$	Ended same as $\eta^1(S)^{TILT}$								
	Vapor Phase			On HOPG					
OptB88-vdw									
$\eta^1(S)^{TILT}$	-21.5		2.75		-24.9		2.61		
π-π (meso)	-23.4			3.35	-23.1			3.40	
π-π (β)	-23.3			3.27	-23.6			3.40	
$\eta^1(S)^{UP}$	-13.1	2.45			-20		2.50		
+ no difference in opti	mized structu	ire values	from starting i	in meso and β	configura	tions			

that the binding energy of phenyl imidazole to CoOEP increases as phenyl imidazole binds to more neighboring molecules. 45,46 We assume that a similar phenomenon is at work in this case as well. In these examples, cooperativity is not the typical view of cooperativity where you see multiple ligands bind to a single receptor. It is instead meant a bit more generally in that adjacent adsorption sites are not independent but influence the binding energy/probability of observing binding at neighboring sites.

Geometrical structures of PhTh-CoOEP complex from DFT calculations. DFT and PW-DFT calculations were performed to identify

potential coordination geometries of PhTh bound to CoOEP adsorbed on graphite and to determine their associated electronic energies of formation. These values are shown in Table 2. Computations were also performed for the complexation of molecular PhTh-CoOEP in phenyloctane for comparison with experimental solution and surface data. The reaction considered was either

PhTh + CoOEP = PhTh-CoOEP, or

PhTh + CoOEP/HOPG = PhTh-CoOEP/HOPG

PW DFT calculations on the isolated PhTh, CoOEP, PhTh-CoOEP molecules and on the HOPG, CoOEP/HOPG and PhTh-CoOEP/HOPG periodic slab structures were conducted. In all the

above calculations the ethyl groups conformation on CoOEP was taken to be in the up position such as to maximize the porphyrin-HOPG contact area.<sup>70</sup> Images of the various optimized structures are presented in Figure 8 and in Supplemental materials.

The  $\pi$ - $\pi$  structure seen in Figure 8c is significantly different from metal bonded ligands we have previously studied. In order to ascertain the role of the crown configuration of the ethyl groups in stabilizing the  $\pi$ - $\pi$  structure, we also performed PW- DFT calculations on the PhThCoP-HOPG system. This allows us to ascertain the importance of the eight ethyl groups. While the detailed orientation of the PhTh relative to the CoP was different, the energies are similar. Thus, the

ethyl groups direct the orientation of the PhTh above the porphyrin, but do not play a major role in the binding. DFT calculations of the electronic energy of formation and the free energy of formation of PhTh-CoOEP yielded different predicted stable geometries depending on functional and method

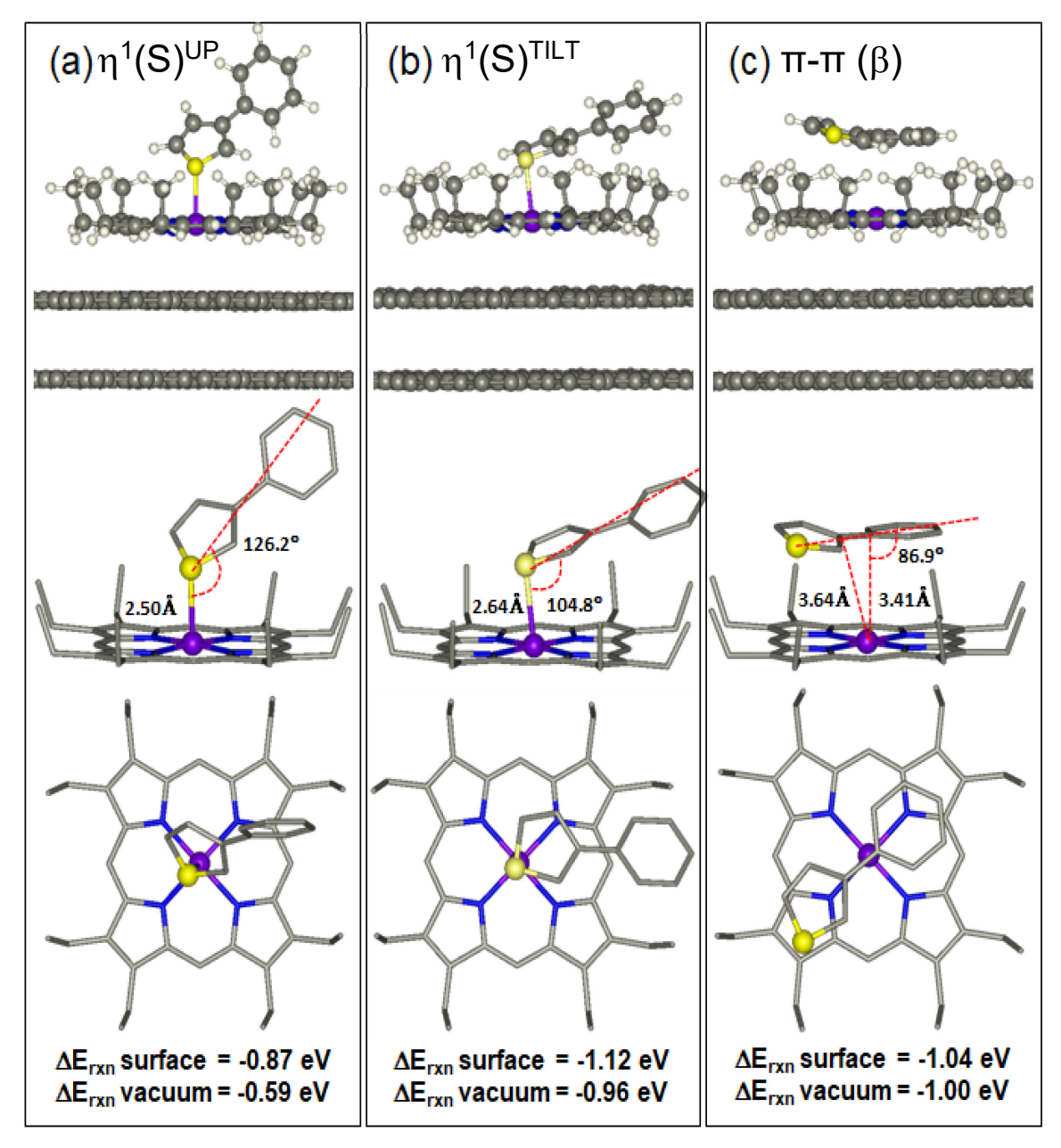


**Figure 8.** Optimized models of PhTh bound to CoOEP absorbed on HOPG based on three different PW-DFT local minima. Each set of results includes a side view of PhTh–CoOEP/HOPG slab in the *ab*-plane of the unit cell (top), geometrical details (bond lengths and angles) of the mode of attachment (middle) and top views of the PhTh–CoOEP adducts emphasizing the different binding positions of PhTh molecule relative to the plane of the porphyrin chromophore (bottom). In both middle and bottom views, the HOPG substate was omitted. Included also are the associated binding energies (in vacuum) of PhTh to the CoOEP/HOPG system and to the free CoOEP.

employed (Table 2). All showed the  $\eta^1(S)$ , Co-S bonded, 'up' configuration (Figure 8a) to be either unstable or least stable in vacuum, liquid, or on HOPG. We thus dismiss this as a possible structure.

The molecular DFT calculations using the B3LYP functional all eventually find a very weak minimum in the energy with the PhTh significantly separated from the CoOEP and  $\Delta G > 0$ . The addition of van der Waals forces (B3LYP-GD3 functional) we identified three local minima in the energy: a tilted  $\eta^1(S)$  structure (Figure 8b) and two energetically similar  $\pi$ - $\pi$  structures. One with the S pointed toward the β positions on the OEP (Figure 8c) and one with it pointed to the meso position (see SI). In solution the B3LYP-GD3 functional has the β oriented structure as slightly lower in energy that any of the others. However, we doubt that these calculations are sufficiently precise to clearly discriminate between the two structures. In this context we have estimated  $\Delta G$  to be near or above +0.3 kcal/mole for the solution phase reaction in PhO. The reader should note that all the Gaussian calculations predict a decrease in the electronic binding energy in going from vapor to solution and a corresponding increase in  $\Delta G$ .

The VASP (optB88-vdw functional) give vapor phase binding energies similar to those predicted by the B3LYP-GD3 functional. In contrast, the energies on HOPG are nearly the same or more negative (more stable) than in the vapor. In the case of the  $\eta^1(S)$  structure it is about 3 kcal more stable on HOPG. Given the Gaussian predictions of decreased stability in solution, these results are consistent with our experimental observation. The complex is more stable on HOPG than in solution.

The tilted Co-S local minimum seen in Figure 8b was found from an initial structure where the thiophene was nearly perpendicular to the porphyrin but the S atom was close to cobalt, similar to Figure 8a. In the  $\eta^1(S)$  structures (Figure 8a and 8b) the calculated Co-S bond lengths are nearly the same, averaging ~2.57 Å. Similar metal-sulfur bond distance of 2.56 Å were reported for rhenium  $\eta^1(S)$  complexes such as for (PPh<sub>3</sub>)<sub>2</sub>Rh(SC<sub>4</sub>H<sub>4</sub>) based on

crystal structure data. 71 The thiophene ring is bent at the sulfur in both PhTh-CoOEP structures shown in figures 8a and 8b with respective tilt angles of 126.2° and 104.8°. Also, the phenyl groupthiophene ring torsional angle (C3-C4-C5-C6, see Figure S5 in the Supporting Information for atom label details) is reduced from 39.2° in the Figure 8a structure to 16.7° in Figure 8b configuration. A common structural feature of all  $\eta^1(S)$  thiophene metal complexes (including substituted thiophenes) is that the metal does not lie in the plane of the thiophene.<sup>1,2,3</sup> The reported tilt angle, the angle between the metal-sulfur-ring plane vector typically varied from about 140° to less than 120° for different transition metals studies (e.g. Re, Ru, Fe, and Ir). 72,73,74 The coordinated sulfur in these complexes was pyramidal and approximately sp<sup>3</sup> hybridized. The tilt angle also has been related to the effective metal-ligand bonding interactions based on the relative overlap between thiophene's bonding  $(\sigma \text{ and } \pi)$  and antibonding  $(\pi^*)$  molecular orbitals and metal d<sub>z2</sub> and d<sub>yz</sub> orbitals.<sup>1,75</sup> The d<sup>5</sup> and d<sup>6</sup> metal tended to form stable thiophene complexes. Cobalt, a d<sup>7</sup> example, on the other hand, exhibited much weaker  $\eta^1(S)$  thiophene coordinating ability than either d<sup>5</sup> or d<sup>6</sup> metals, generally resulting in thiophene ring opening (i.e. C-S bond cleavage) and Co–C bond insertion reaction. 1,50,76 When strong electron donors were simultaneously bound to the transition metal center, thiophene acted as an acceptor leading to stronger metal-thiophene binding.<sup>3,77</sup> Our calculated PhTh-CoEOP binding profile (based on the optB88-vdw functional) predicts a stable  $\eta^1(S)$  ligand coordination mode. Lower binding for the on-surface complexes (Figure 8a and c) also supports a strong electronic contribution from the HOPG substrate stabilizing the  $\eta^1(S)$  complex. However, this same optB88-vdw functional also predicts an unusual yet stable  $\pi$ - $\pi$ complex (Figure 8c).

In Figure 8c, the PhTh ligand is shown to lie nearly parallel to the porphyrin chromophore and there is no cobalt-sulfur bond. The initial structure in this optimization was based on the lowest energy configuration in the gas phase found using the B3LYP-GD3 functional. This geometrical arrangement is suitable for the Co<sup>2+</sup> ion to bind to ligand via the 2,3 carbon atoms ( $\eta^2$ ) mode in both the free and the surface supported complex (see Figure S5). However, the calculated Co-C distances are too long to support a stable  $\eta^2(C=C)$  complex: Co-C(4) = 3.64 Å and Co-C(5) = 3.41 Å. Anaverage Co-C bond distance in neutral arene complexes is ~2.1Å. This unexpected parallel arrangement of the aromatic ligand and the CoOEP chromophore combined with their large separation distance ( $\sim$ 3.4 Å) suggests that noncovalent  $\pi$ – $\pi$ bonding is probably responsible for the predicted geometry of the PhTh-CoEOP complex. Typical reported distances for  $\pi$ - $\pi$  interactions are 3.3-3.8

Intriguingly, the results of our calculations give no clear prediction of the final product structure. The tilted  $\eta^1(S)$  structure (Figure 8b) has the most negative electronic reaction energy on HOPG and a large decrease in the electronic energy in going from the gas phase to the surface. This suggest it is the dominant geometry; however, it does not rule out that the other  $\pi$ - $\pi$  structures may coexist or be in thermal equilibrium. One must still consider the structure of the phenylthiophene complex an open question.

A single PhTh binding per CoOEP is assumed because related thiophene metal porphyrin complexes have been reported to be 1:1 complexes. For example, the thiophene cobalt(II)tetraphenyl porphyrin complex <sup>19,26</sup> and the thiophene Ruthenium(II)tetraphenyl porphyrin complex <sup>19</sup> both are reported to have one thiophene per porphyrin.

One clear outcome of the calculations is that the surface complex is more stable than the solution complex. We are currently attempting to produce high resolution images at reduced temperature in order to definitively resolve the issue of PhTh-CoOEP complex structure.

#### **CONCLUSIONS**

Using single molecule microscopy, demonstrated an in-situ study of a simple thiophene ligand binding reversibly to cobalt porphyrin at the solution/solid interface at room temperature. Programs to assist in analyzing the large data sets are provided. Combined results from experiments and DFT computations allowed us to rationalize cooperative interporphyrin interactions and the importance of the HOPG substrate. Thermodynamic data derived from STM imaging was effectively modeled by the Langmuir isotherm, but it is likely that this is only because the coverage range studied is low and the variation in adsorption energy with number of adjacent occupied sites is a small fraction of the adsorption energy. In this regime cooperative adsorption isotherms like the Temkin isotherm are Thus, the single molecule equally good fits. analysis method presented here is significantly more sensitive to cooperative behavior than is isotherm fitting.

PW-DFT calculations generated two potential binding geometries of PhTh to CoOEP: Co-S bonded ligand and noncovalent  $\pi$ - $\pi$  interactions with a parallel arrangement of the aromatic ligand and the CoOEP/HOPG. Computed binding energies for the PhTh-CoOEP system were found to depend strongly on the DFT functional and the support. As might be expected, the addition of van der Walls terms in the potential significantly stabilizes the PhTh-CoOEP complex. Moreover, the unexpected noncovalent  $\pi$ - $\pi$  configuration is strongly stabilized by the HOPG surface interactions. This result corroborates the electronic influence importance of the HOPG substrate in regulating ligand biding affinity as well as geometry.

Overall, thiophene complexation reactions are important in a variety of fields from transportation fuels to medicine. This study shows how a heterogeneous environment like the solution/solid interface can provide stabilization to a complex. The high-resolution, quantitative knowledge gained at the molecular level combined with theoretical studies offer insights into the nature of chelation and cooperativity at interfaces. It also suggests additional control parameters for improved

selectivity and sensitivity of sensors, catalysts, and surface driven synthesis that can be applied beyond the specific system described here. The implications are that a surface should be exploited for its capacity to influence complexation products stability and geometry in order to improve processes such as catalysis and sensing.

## **ACKNOWLEDGMENTS**

We are grateful to the National Science Foundation for supporting this work under grant no. CHE-1800070. Computational work is performed using resources from the Center for Institutional Research Computing (CIRC) at Washington State University (WSU). The authors gratefully acknowledge Jake Bailey for his assistance in acquiring electronic spectra and cooperativity data analysis.

## **AUTHOR INFORMATION**

# **Corresponding Authors**

**Ursula Mazur** - Department of Chemistry, Washington State University, Pullman, Washington 99164-4630, United States; orcid.org/0000-0002-3471-4883; Email: umazur@ wsu.edu

**K. W. Hipps** – Department of Chemistry, Washington State University, Pullman, Washington 9164-4630, United States; Email: hipps@wsu.edu orcid.org/0000-0002-5944-5114

## Authors

Kristen N. Johnson – Department of Chemistry, Washington State University, Pullman, Washington 99164-4630, United States; orcid.org/0000-0002-7452-9973

Shammi Rana – Department of Chemistry, Washington State University, Pullman, Washington 99164-4630, United States; orcid.org/0000-0002-9058-8500

Bhaskar Chilukuri- Department of Chemistry, Illinois State University, Normal, Illinois 61790, United States; orcid.org/0000-0002-7452-9973 orcid.org/0000-0002-7452-9973

Complete contact information is available at: https://pubs.acs.org/10.1021/acs.jpcc.0c05516 orcid.org/0000-0002-5944-5114; Email:

## **Author Contributions**

+ K.N.J and S.R, contributed equally

## **Notes**

The authors declare no competing financial interest.

# ASSOCIATED CONTENT

# **Supporting Information**

The Supporting Information is available free of charge at https://pubs.acs.org/doi/10.1021/acs.jpcc.0c05516. Additional experimental details and methods; UV-visible spectra of CoOEP and PhTh-CoOEP solutions; STM image of CoOEP prior to PhIm addition; STM images showing stability of the CoOEP monolayer and adduct over time, transition statistics for "blinking" of CoOEP; experimental and theoretical fractions of molecules with k dark nearest neighbors versus p; computational modeling (PW-DFT) details and structural parameters.

## REFERENCES

\_

- (1) Angelici, R. J. Thiophenes in Organotransition Metal Chemistry: Patterns of Reactivity. *Organometallics* **2001**, *20*, 1259–1275.
- (2) Rauchfuss, T. B. The Coordination Chemistry of Thiophenes. *In Progress in Inorganic Chemistry*, Vol. 39; Lippard, S. J., Ed.; John Wiley & Sons, Inc., 1991; 259–329.
- (3) Harris, S. Understanding the Binding and Activation of Thiophenic Molecules in Transition Metal Complexes and Clusters. *Polyhedron*, **1997**, *16*, 3219-3233.
- (4) Transition Metal Sulphides: Chemistry and Catalyis. Weber, T.; Prins, R.; van Santen, R. A. Eds.; Kluwer Academic Publishing, Netherlands. 1998.
- (5) Salazar, N.; Rangarajan, S.; Rodríguez-Fernandez, J.; Mavrikakis, M.; Lauritsen, J. V. Site-dependent Reactivity of MoS<sub>2</sub> Nanoparticles in Hydrodesulfurization of Thiophene. *Nat. Commun.* **2020**, *11*, 4369.
- (6) Flores, M.; Cisternas E.; Mella, A.; Jullianc, A.S. Nunez, D.; Soler, M. Adsorption of 2-thiophene Curcuminoid Molecules on an Au(111) Surface. *Appl. Surf. Sci.* **2018**, *427*, 620–625.
- (7) Maksimov, A. L.; Nekhaev, A. I. Complexation of Thiophene Compounds with Transition Metals as the Key to Understanding the Mechanisms of Desulfurization of Petroleum Products (Review). *Pet. Chem.* **2020**, *60*, 155–165.
- (8) Tran, D. T.; Palomino, J. M.; Oliver, S. R. J. Desulfurization of JP-8 Jet Fuel: Challenges and Adsorptive Materials. *RSC Adv.* **2018**, *8* (13), 7301–7314.
- (9) Brorson, M.; Carlsson, A.; Topsoe, H. The Morphology of MoS<sub>2</sub>, WS<sub>2</sub>, Co–Mo–S, Ni–Mo–S and Ni–W–S Nanoclusters in

- Hydrodesulfurization Catalysts Revealed by HAADF-STEM. Catal. Today 2007, 123, 31-36.
- (10) Baubet, B.; Girleanu, M.; Gay, A. S.; Taleb, A. L.; Moreaud, M.; Wahl, F.; Delattre, F.; Devers, L.; Hugon, A.; Ersen, O.; Afanasiev, P.; Raybaud, P. Quantitative Two-dimensional (2D) Morphology-selectivity Relationship of CoMoS Nanolayers: a Combined High-resolution High-angleannular Dark Field Scanning Transmission Electron Microscopy (HR HAADF-STEM) and Density Functional Theory (DFT) Study. *ACS Catal.* **2016**, *6*, 1081–1092.
- (11) Tanimu, A. Alhooshani, K. Advanced Hydrodesulfurization Catalysts: A Review of Design and Synthesis. *Energy Fuels* **2019**, *33*, 2810–2838.
- (10) DePillis, G. D.; Decatur, S. M; Barrick, D.; Boxer, S. G. Functional Cavities in Proteins: A General Method for Proximal Ligand Substitution in Myoglobin. *J. Am. Chem. Soc.* **1994**, *116*, 6981-6982.
- (13) Desai, S.B.; Desai, P.B.; Desai, K.R. Synthesis of some Schiff Bases, Thiazolidinones and Azetidinones Derived from 2,6-diaminobenzo1,2-d: 4,5-d' bisthiazole and their Anticancer Activities. *Heterocycl. Commun*, **2001**, 7, 83–90.
- (14) Harpstrite, S. E.; Collins, S. D.; Oksman, A; Goldberg, D. E.; Sharma, V. Synthesis, Characterization, and Antimalarial Activity of Novel Schiff-base-phenol and Naphthaleneamine Ligands. *Med. Chem.* **2008**, *4*,392–395.
- (15) Yasmeen, S.; Sumrra, S. H.; Akram, M. S.; Chohand, Z. H. Antimicrobial Metal-based Thiophene Derived Compounds. *J. Enzyme Inhib. Med. Chem.* **2017**, *32*, 106–112.
- 16 Li, L. X.; Xie, Z. H.; Fernandez, C.; Wu, L.; Cheng, D.; Jiang, Z. H.; Zhong, C. J. Development of a Thiophene Derivative Modified LDH Coating for Mg Alloy Corrosion

- Protection. *Electrochem. Acta* **2020**, 1/135186-12/135186.
- (17) Guo,1L.; Safi, Z. s.; Kaya, S.; Shi, W.; Tuzun, B.; Altunay, N.; Kaya, C. Anticorrosive Effects of Some Thiophene Derivatives Against the Corrosion of Iron: A Computational Study. *Front Chem.*, **2018**, *6*, 1/155-11/155.
- (18) Liang, Z.; Thomas, C. W. Mak. Silver(I)—Thiophene  $\pi$  Interaction in the Assembly of Coordination Networks with the Supramolecular Synthons R–C:C $\supset$ Ag<sub>n</sub> (R = 2-or 3-thienyl; n = 4). Organometallics **2007**, 26, 4439-4448.
- (19) Brunink, J. A. J.; Di Natale, C.; Bungaro, F.; Davide, F. A. M.; D'Amico, A.; Paolesse, R.; Boschi, T.; Faccio, M.; Ferri, G. The Application of Metalloporphyrins as Coating Material for Quartz Microbalance-Based Chemical Sensors. *Anal. Chim. Acta* **1996**, *325*, 53–64.
- (20) Shah, R.; Verma, P. K. Therapeutic Importance of Synthetic Thiophene. *Chem. Central J.* **2018**, 137.
- (21) Pathania, S.; Narang, R. K.; Rawal, R. K. Role of Sulphur-Heterocycles in Medicinal Chemistry: An Update. *Eur. J. Med. Chem.* **2019**, 486–508.
- (22) Sadimenko, A. P. Organometallic Compounds of Furan, Thiophene, and Their Benzannulated Derivatives. *Adv. Heterocycl. Chem.* **2001**, *78*, 1–64.
- (23) Elfeninat, F.; Fredriksson, C.; Sacher, E.; Selmani, A. A Theoretical Investigation of the Interactions between Thiophene and Vanadium, Chromium, Copper, and Gold. *J. Chem. Phys.* **1995**, 102, 6153-6158.
- (24) Ding, Y.; He, M.; Niu, Y.; Wang, D.; Cui, Y.; Feng, S. Electronic Structures of Bis- and Monothiophene Complexes with Fe, Co, Ni: A Density Functional Theory Study. *J. Phys. Chem. A* **2009**, 113, 10291–10298.
- (25) Atesin, T. A.; Jones, W. D. A Deeper Look into Thiophene Coordination Prior to Oxidative Addition of the C-S Bond to Platinum(0): A

- Computational Study Using DFT and MO Methods. *Organometallics* **2008**, 27, 53–60.
- (26) Pezeshk, A.; Davison, P. E.; Greenaway, F. T. EPR of Axial Adducts of Cobalt(II) Tetraphenylporphyrin. *Inorg. Nucl. Chem. Lett.* **1980**, *16*, 105–107.
- (27) Yik, E.; Iglesia, E. Mechanism, and Site Requirements for Thiophene Hydrodesulfurization on Supported Re Domains in Metal or Sulfide Form *J. Catal.* **2018**, *368*, 411–426.
- (28) Chen, L.; Xu, Y.; Wang, B.; Yun, J.; Dehghan, F.; Xie, Y.; Liang, X. Mg-modified CoMo/Al<sub>2</sub>O<sub>3</sub> with Enhanced Catalytic Activity for the Hydrodesulfurization of 4, 6-dimethyldibenzothiophene. *Catal. Commun.*, **2021**, *155*, 1/106316-5/106316.
- (29) Hensen, E. J. M.; Vissenberg, M. J.; de Beer, V. H. J.; van Veen, J. A. R.; van Santen, R. A. Kinetics and Mechanism of Thiophene Hydrodesulfurization over Carbon-Supported Transition Metal Sulfides. *J. Catal.*, **1996**, *163*, 429–435.
- (30) Mahmoudabadi, Z. S.; Tavasoli, A. Rashidi, A.; Esrafili, M. Catalytic Activity of Synthesized 2D MoS<sub>2</sub>/graphene Nanohybrids for the Hydrodesulfurization of SRLGO: Experimental and DFT study. *Envir. Sci. Pollut. R.*, **2021**, *28*, 5978–5990
- (31) Daage, M.; Chianelli, R. R. Structure-Function Relations in Molybdenum Sulfide Catalysts: the "Rim-edge" Model. *J. Catal.* **1994**, *149*, 414–427.
- (32) Castillo-Villalon, P; Ramirez, J.; Castaneda, R. Relationship Between the Hydrodesulfurization of Thiophene, Dibenzothiophene, and 4,6-dimethyl dibenzothiophene and the Local Structure of Co in Co–Mo–S Sites: Infrared Study of Adsorbed CO. J. Catal. 2012, 294, 54–62.
- (33) Liu, D.; Li, Z.; Sun, Q.; Kong, X.; Zhao, A.; Wang, Z. In situ FT-IR study of thiophene

- adsorbed on the surface of sulfided Mo catalysts. *Fuel*, **2012**, *92*, 77–83.
- (34) Edwards, J. C.; Adams, R. D.; Ellis, P. D. A <sup>95</sup>Mo Solid-state NMR Study of Hydrodesulfurization Catalysts. 1. Formation of Fresh HDS Catalyst Precursors by Adsorption of Polyoxomolybdates onto γ-Alumina. *J Am. Chem. Soc.* **1990**, *112*, 8349-8364.
- (35) Hagiwara, K.; Ebihara, T.; Urasato, N.; Fujikawa, T. Application of <sup>129</sup>Xe NMR Spectroscopy to Analysis of CoMo/Al<sub>2</sub>O<sub>3</sub> Hydrodesulfurization Catalyst-Effect of Sulfidation on <sup>129</sup>Xe NMR Spectra. *J. Japan Petroleum Institute*, **2007**, *50*, 139-146.
- (36) Du, S.; Li, T.; Wang, X.; Zhang, L.; Yang, Z.; Lin, R.; Zhu, T. Molecular Simulation on Mechanism of Thiophene Hydrodesulfurization on Surface of Ni<sub>2</sub>P. *Energy Explor. Exploit.*, **2021**, *39*, 975–992.
- (37) Sorescu, D. C.; Sholl, D. S.; Cugini, A. V. Density Functional Theory Studies of Chemisorption and Diffusion Properties of Ni and Ni-Thiophene Complexes on the MoS<sub>2</sub> Basal Plane. *J. Phys. Chem. B* **2003**, *107*, 1988-2000.
- (38) Noh, J.; Ito, E.; Nakajima, K.; Kim, J.; Lee, H.; Hara, M. High-Resolution STM and XPS Studies of Thiophene Self-Assembled Monolayers on Au(111). *J. Phys. Chem. B* **2002**, *106*, 7139-7141.
- (39) Mathieu Linares, M.; Scifo, L.; Demadrille, R.; Brocorens, P.; Beljonne, D.; Lazzaroni, R.; Grevin, B. Two-Dimensional Self-Assemblies of Thiophene-Fluorenone Conjugated Oligomers on Graphite: A Joint STM and Molecular Modeling Study. *J. Phys. Chem. C* **2008**, *112*, 6850-6859.
- (40) Gottfried, J. Michael. Surface Chemistry of Porphyrins and Phthalocyanines, *Surface Sci. Rep.* **2015**, 70, 259-379.
- (41) Otsuki, J. STM Studies on Porphyrins. *Coord. Chem. Rev.* **2010**, *254*, 2311-2341.

- (42) Johnson, K. N.; Chilukuri, B.; Fisher, Z. E.; Hipps, K. W.; Mazur, U. Role of the Supporting Surface in the Thermodynamics and Cooperativity of Axial Ligand Binding to Metalloporphyrins at Interfaces. *Current Org. Chem.* **2022**, 26, 553-662.
- (43) Johnson, K. N.; Hipps, K. W.; Mazur, U. Mazur. Quantifying Reversible Nitrogenous Ligand Binding to Co(II) Porphyrin Receptors at the Solution/Solid Interface and in Solution. *Phys. Chem. Chem. Phys.*, **2020**, 22, 24226–24235.
- (44) Mazur, U.; Hipps, K. W. Single Molecule Level Studies of Reversible Ligand Binding to Metal Porphyrins at the Solution/solid Interface. *J. Porph. Phthal.* **2020**, *24*, 993–1002.
- (45) Nandi, G.; Chilukuri, B.; Hipps, K. W.; U. Surface Directed Mazur, Reversible **Imidazole** Ligation to Nickel(II) octaethylporphyrin at the Solution/Solid Interface: A Single Molecule Level Study. Phys. Chem. Chem. Phys. 2016, 18, 20819–20829.
- (46) Korpany, K. V.; Chilukuri, B.; Hipps, K. W.; Mazur, U. Cooperative Binding of 1-Phenylimidazole to Cobalt(II) octaethylporphyrin on Graphite: A Quantitative Imaging and Computational Study at Molecular Resolution. *J. Phys. Chem. C*, **2020**, *124*, 18639–18649.
- (47) Friesen, B. A.; Bhattarai, A.; Mazur, U.; Hipps, K. W. Single Molecule Imaging of Oxygenation of Cobalt Octaethylporphyrin at the Solution/Solid Interface: Thermodynamics from Microscopy. *J. Am. Chem. Soc.* **2012**, 134, 14897–14904.
- (48) Visser, J.; Katsonis, N.; Vicario, J.; Feringa, B. L. Two-Dimensional Molecular Patterning by Surface-Enhanced Zn-Porphyrin Coordination. *Langmuir* **2009**, *25*, 5980–5985.
- (49) Zhou, X. Y.; Xu, C.; Guo, P. P.; Sun, W. L.; Wei, P. J.; Liu, J. G. Axial Ligand Coordination Tuning of the Electrocatalytic Activity of Iron Porphyrin Electrografted onto Carbon Nanotubes

- for the Oxygen Reduction Reaction. *Chem. A Eur. J.* **2021**, *27*, 9898–9904.
- (50) Ding, Y.; He, M.; Niu, Y.; Wang, D.; Yan Cui, Y.; Feng, S. Electronic Structures of Bisand Monothiophene Complexes with Fe, Co, Ni: A Density Functional Theory Study. *J. Phys. Chem. A* **2009**, *113*, 10291–10298.
- (51) Kresse, G.; Furthmüller, J. Efficiency of Ab-Initio Total Energy Calculations for Metals and Semiconductors Using a Plane-Wave Basis Set. *Comput. Mater. Sci.* **1996**, *6*, 15–50.
- (52) Kresse, G.; Hafner, J. Ab Initito Molecular Dynamics for Liquid Metals. *Phys. Rev. B* **1993**, 47, 558-561. 8
- (53) Gaussian 16, Revision C.01, Gaussian, Inc., Wallingford CT, 06492, **2013**.
- (54) Foresman, J.; Frisch, A. *Exploring Chemistry with Electronic Structure Methods*3rd ed.; Gaussian Inc., Wallingford, CT. **2015**.
- (55) Kresse, G.; Joubert, D. From Ultrasoft Pseudopotentials to the Projector Augmented-Wave Method. *Phys. Rev. B* **1999**, *59*, 1758,.
- (56) Blöchl, P. E. Projector Augmented-Wave Method. *Phys. Rev. B* **1994**, *50*, 17953.
- (57) Klime, J.; Bowler, D. R.; Michaelides, A. van der Waals Density Functionals Applied to Solids *Phys. Rev. B Condens. Matter Mater. Phys.*, **2011**, *83*, 195131.
- (58) Becke, A.D.; Density-functional exchangeenergy approximation with correct asymptotic behavior. *Phys. Rev. A*, 1988, 38, 3098–3100.
- (59) Nandi, G.; Chilukuri, B.; Hipps, K.W.; Directed Mazur, U. Surface Reversible **Imidazole** Ligation to Nickel(II) Octaethylporphyrin the at Solution/solid Interface: a Single Molecule Level Study. Phys. Chem. Chem. Phys. 2016, 18, 20819–20829.
- (60) Jahanbekam, A.; Chilukuri, B.; Mazur, U.; Hipps, K. W. Kinetically Trapped Two-Component Self-Assembled Adlayer. *J. Phys. Chem. C* **2015**, *119*, 25364–25376.

- (61) Chilukuri, B.; Mazur, U.; Hipps, K. W. Effect of Dispersion on Surface Interactions of Cobalt(II) Octaethylporphyrin Monolayer on Au(111) and HOPG(0001) Substrates: A Comparative First Principles Study. *Phys. Chem. Chem. Phys.* **2014**, *16*, 14096–14107.
- (62) Borders, B.; Adinehnia, M.; Chilukuri, B.; Ruf, M.; Hipps, K. W.; Mazur, U. Tuning the Optoelectronic Characteristics of Ionic Organic Crystalline Assemblies. *J. Mater. Chem. C* **2018**, 6, 4041–4056.
- (63) Adinehnia, M.; Borders, B.; Ruf, M.; Chilukuri, B.; Hipps, K. W.; Mazur, U. Comprehensive Structure–Function Correlation of Photoactive Ionic π-Conjugated Supermolecular Assemblies: An Experimental and Computational Study. *J. Mater. Chem. C* **2016**, *4*, 10223–10239.
- (64) Zhang, Y. C.; Chilukuri, B.; Hanson, T. B.; Heiden, Z. M.; Lee, D. Y. Connecting Solution-Phase to Single-Molecule Properties of Ni(Salophen). *J. Phys. Chem. Lett.* **2019**, *10*, 3525–3530.
- (65) Korpany, K. V.; Chilukuri, B.; Hipps, K. W.; Mazur, U. Cooperative Binding of 1-Phenylimidazole to Cobalt(II) octaethylporphyrin on Graphite: A Quantitative Imaging and Computational Study at Molecular Resolution. *J. Phys. Chem. C*, **2020**, *124*, 18639–18649.
- (66) Johnson, K. N.; Mazur, U.; Hipps, K. W. Single-Molecule Kinetic Analysis of Oxygenation of Co(II) Porphyrin at the Solution/Solid Interface. *J. Phys. Chem. Lett.* **2022**, *13*, 4918-4923.
- (67) Temkin, M. On Heterogeneous Surfaces with Interaction Between Adsorbate Molecules. *Zh. Fiz. Kh.* **1941**, *15*, 296-332.
- (68) Foo, K. Y.; Hameed, B.H. Insights into the Modeling of Adsorption Isotherm Systems, *Chem. Eng. J.* **2010**, *156*, 2-10.
- (69) Pettitt, A. N.; Stephens, M. A. The Kolmogorov-Smirnov Goodness-of-Fit Statistic

- with Discrete and Grouped Data. *Technometrics* **1977**, *19* (2), 205–210.
- (70) Scudiero, L.; Barlow, D. E.; Hipps, K. W. Scanning Tunneling Microscopy, Orbital-Mediated Tunneling Spectroscopy, and Ultraviolet Photoelectron Spectroscopy of Nickel(II) Octaethylporphyrin Deposited from Vapor. J. Phys. Chem. B, 2002, 106, 996-1003.
- (71) Sanchez-Delgado, R. A.; Marquez-Silva, R. L.; Puga, J.; Tiripicchio, A.; Tiripicchio, C. *J. Organometal. Chem.*, **1986**, *316*, C35.
- (72) Angelici, R. J. Structural Aspects of Thiophene coordination in Transition Metal Complexes. *Coord. Chem. Rev.*, **1990**, *105*, 61-76.
- (73) Sanchez-Delgado, R. A. Coordination and Activation of Thiophenes in Metal Complexes. *Catalysis by Metal Complexes*. **2002**, *24*, 35-61.
- (74) Rao, K. M.; Day, C. L.; Jacobson, R. A.; Angelici, J. R.  $\eta^1(S)$  and  $\eta^6$  coordination of dibenzothiophene (DBT) in Cp\*MC1<sub>2</sub>[ $\eta^1(S)$ -DBT] and Cp'M( $\eta^6$  DBT)<sup>2+</sup> (M = Ir, Rh). *Inorg. Chem.*, **1991**, *30*, 5046-5049.
- (75) Angelici, R. J. Organometallic Complexes as Models for the Adsorption of Thiophenes on Hydrodesulfurization (HDS) Catalyts. *Bull. Soc. Chim. Belg.*, **1995**, *104*, 265-282.
- (76) Jones, W. D.; Chin, R.M. Thiophene Carbon-Sulfur Bond Cleavage by Cobalt. Synthesis, Structure, and Dynamics of [(C<sub>5</sub>Me<sub>5</sub>Co]<sub>2</sub>(C<sub>4</sub>H<sub>4</sub>S). *Organometallics*, **1992**, *11*, 2698-2700.
- (77) Eissa, H.; Shaalan, N.; Mahde, S. Synthesis, Characterization, Thermodynamic and Biological Activity Studies for New Complexes of Some Transition Metals and Zinc with Schiff's Bases [2,5di(1-Thi-Ophen-2-yl-Ethylidene)-Hydrazine) 1,3,4-Thiadiazole]. *Org. Med. Chem., I. J.,* **2018**, *5*, 001-005.
- (78) Hays, M. L.; Hanusa, T. P. Substituent Effects as Probes of Structure and Bonding in

- Mononuclear Metallocenes. *Adv. Organometallic Chem.*, **1996**, *40*, 117-170.
- (79) Janiak, C. A Critical Account on Stacking in Metal Complexes with aromatic nitrogen-containing ligands. *Dalton Trans.*, **2000**, 3885–3896.
- (80) Alvarez, S. A Cartography of the van der Waals Territories. *Dalton Trans.*, **2013**, *42*, 8617-8636.

